ELSEVIER

Contents lists available at ScienceDirect

Organic Electronics

journal homepage: www.elsevier.com/locate/orgel





Color-temperature dependence of indoor organic photovoltaic performance

Boya Zhang ^a, Justin C. Bonner ^a, Lakshmi N.S. Murthy ^a, Thien A. Nguyen ^b, Fong-Yi Cao ^c, Yen-Ju Cheng ^c, Behrang H. Hamadani ^d, Julia W.P. Hsu ^a, ^{*}

- ^a Department of Materials Science and Engineering, University of Texas at Dallas, Richardson, TX, 75080, United States
- ^b Department of Bioengineering, University of Texas at Dallas, Richardson, TX, 75080, United States
- ^c Department of Applied Chemistry, National Yang Ming Chiao Tung University, Hsinchu, 30010, Taiwan
- ^d National Institute of Standards and Technology, Gaithersburg, MD, 20899, United States

ARTICLE INFO

Keywords: Indoor light harvesting Organic photovoltaics Absorption effect Power conversion efficiency Correlated color temperature

ABSTRACT

Organic materials are uniquely suited for indoor light energy harvesting because they absorb mostly in the visible spectrum and the absence of ultraviolet light minimizes their degradation. However, the performance of photovoltaic devices under indoor lighting depends on the correlated color temperatures (CCTs) of the light sources but has not been examined previously. Here we study organic photovoltaics with different combinations of donor and acceptor materials under white light-emitting diode (LED) illumination. The current density – voltage (J - V) measurements were performed under illuminance of 1000 lx at nominal LED CCTs of 3000 K, 4000 K, and 6000 K. Absorption spectra of neat and blended films and device external quantum efficiency were measured. Our results show that active layer absorption in the blue LED emission region determines the short-circuit current density (J_{sc}) increase from 3000 K to 6000 K CCT; the more the active layer absorbs at 450 nm, the larger the J_{sc} increase under higher CCTs. We find that the normalized fractional absorption of the active layer at 450 nm needs to be > 0.85 to eliminate a decrease in power conversion efficiency as the CCT is varied from 3000 K to 6000 K. This work highlights the unique tunability of organic absorbers that is difficult to achieve in inorganic materials and provides guidance on how to select organic absorbers for specific applications under different indoor illumination conditions.

1. Introduction

The Internet of things (IoTs) enhances the quality of human life as users benefit from widespread smart applications, such as monitoring of home security and energy usage, intelligent traffic light switching, and remote recording of health status [1]. Many IoT microelectronic devices—sensors, actuators, and wearable devices—are small, lightweight, and mobile, making wired sources or batteries impractical for powering these devices [2]. Alternative energy sources, such as thermal, mechanical, and light energy harvesters, are being explored to power small wireless IoT devices [3]. Among them, indoor light energy harvesters (photovoltaics) are very attractive owing to the omnipresence of indoor lighting [4,5]. They exhibit higher power conversion efficiency (PCE) and enhanced operational life than used in outdoor panels owing to less temperature and humidity variation, low illumination intensity, and no presence of ultraviolet/infrared radiation in the light source [6]. Indoor photovoltaics are promising to power IoT devices and low-energy

consuming electronics, such as basic calculators, kitchen weighing scales, and wearables, because they can satisfy the energy needs using small cm²-size cells [7]. As the power to operate the wireless sensor networks continues decreasing, the type and number of nodes powered by indoor photovoltaics are rapidly increasing, leading to significant market growth [7]. Among various indoor photovoltaic technologies [5], devices that employ organic absorbers are uniquely promising due to their high absorption coefficient, bandgap tunability, mechanical flexibility, and good spectral match with artificial light sources [8]. Because of these exceptional advantages, research has been active in the field of indoor organic photovoltaics (IOPVs), which convert the light energy from various indoor light sources directly into electricity [8–12].

Among artificial light sources, light-emitting diodes (LEDs), with superior features of low cost, long lifetime, and low power consumption, are the most commonly used today [13,14]. Common LEDs emit in two spectral regions: the blue region with a narrow peak centered at \approx 450 nm and the red region with a broad peak centered at \approx 600 nm [15]. The

E-mail address: jwhsu@utdallas.edu (J.W.P. Hsu).

^{*} Corresponding author.

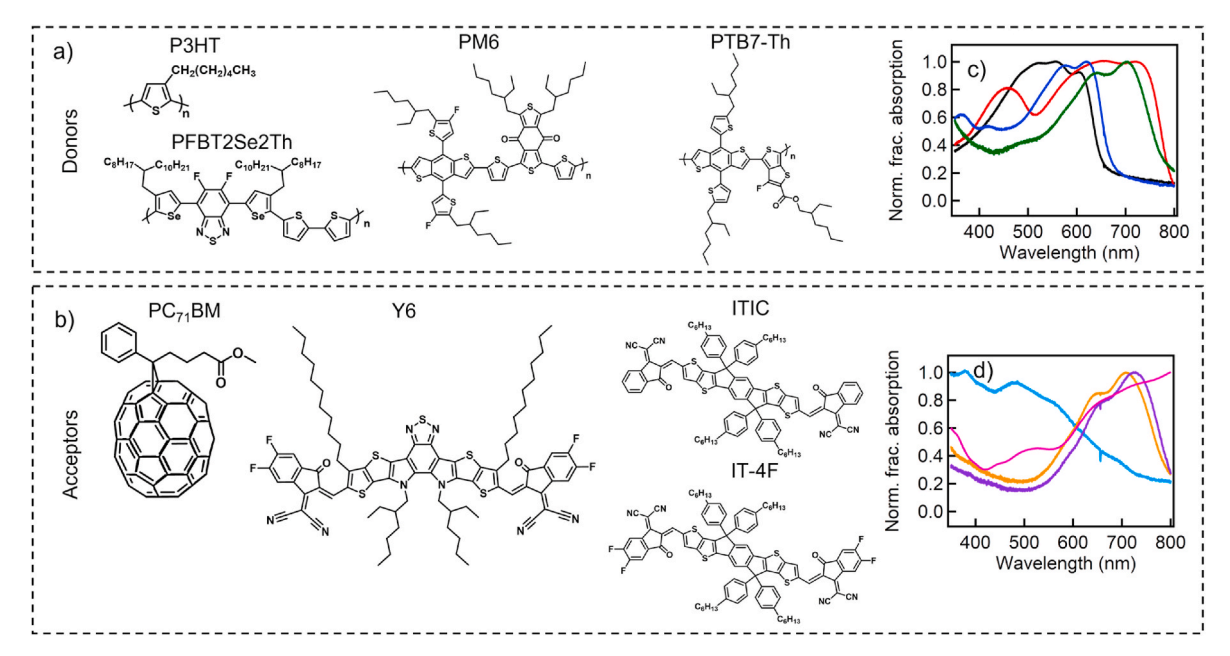


Fig. 1. Chemical structures of (a) donors (P3HT, PFBT2Se2Th, PM6, and PTB7-Th) and (b) acceptors (PC₇₁BM, Y6, ITIC, and IT-4F). Norm-frac-abs spectra of (c) donors (P3HT (black), PFBT2Se2Th (red), PM6 (navy blue), and PTB7-Th (green)) and (d) acceptors (PC₇₁BM (light blue), Y6 (pink), ITIC (orange), and IT-4F (purple)). (For interpretation of the references to color in this figure legend, the reader is referred to the Web version of this article.)

intensity ratio between the blue and red regions determines an LED's correlated color temperatures (CCTs) [15], which is the temperature of a blackbody radiator whose perceived color is nearly the same as the lighting source even though the spectral distribution of the source significantly differs from that of the blackbody [16]. LEDs with higher CCTs have a stronger optical emission in the blue region [17]; hence, LEDs with CCTs below 3300 K are commonly referred to as 'warm white', 3300 K–5300 K as 'intermediate neutral', and above 5300 K as 'cool white' [18]. 'Warm white' LEDs are preferred for relaxing environments, such as living rooms and bedrooms in residential homes, because they induce a sense of relaxation or calm emotion [19]. On the contrary, 'cool white' LEDs are preferred for working environments, such as classrooms and offices, because blue light increases people's level of alertness [19].

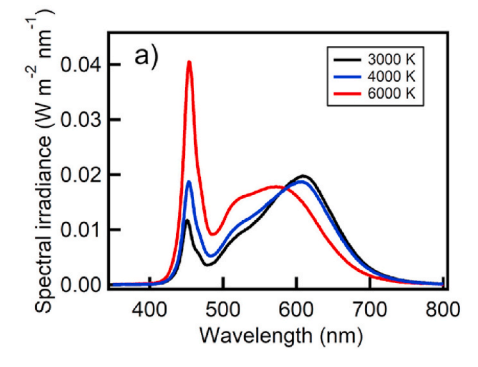
For a given illuminance (lx), the measure of the intensity as perceived by the human eye, 'cool white' LEDs emit a higher light intensity (irradiance, W m $^{-2}$). The higher intensity boosts the short-circuit current density (J_{sc}) in photovoltaic (PV) devices, but the PCE can be lower because the increase in generated power density is smaller than the increase in the light intensity. Hamadani et al. reported that PCEs for several common inorganic PVs are all reduced when CCT increases from 3000 K to 6000 K [15]. Similarly, Yin et al. reported a PCE reduction in an organic bulk heterojunction (BHJ) IOPV from 3000 K to 6500 K CCT [17]. To achieve equal or greater PCEs under 'cool white' as compared to

under 'warm white' LEDs, the match between the active layer absorption with respect to the LED emission spectra needs to be carefully considered so that the $J_{\rm SC}$ increase is large enough to compensate for the higher intensity of the 'cool white' LEDs. However, to the best of our knowledge, there is no report that quantifies the absorption spectrum and relates it to the $J_{\rm SC}$ and PCE changes from 'warm white' to 'cool white' illumination. Hence, we conduct a careful and quantitative examination under different CCTs to study how organic active layer absorption affects device $J_{\rm SC}$ and PCE.

Here we study eight organic absorbers with different combinations of donor and acceptor materials. The IOPV devices are measured under an LED source at nominal 3000 K, 4000 K, and 6000 K CCTs with a fixed illuminance of 1000 lx. We find that the more the active layer absorbs in the blue region, the larger the $J_{\rm sc}$ increase from CCT of 3000 K–6000 K. Our results establish a criterion based on active layer absorption at 450 nm to ensure that PCE is maintained when switching from 'warm white' to 'cool white' LEDs. This work provides guidance on how to select organic absorbers for IOPV performance specific to applications under different CCTs.

2. Results and discussion

Fig. 1 shows the chemical structures (Fig. 1a and b) and normalized fractional absorption (Norm-frac-abs) spectra (Fig. 1c and d) of four



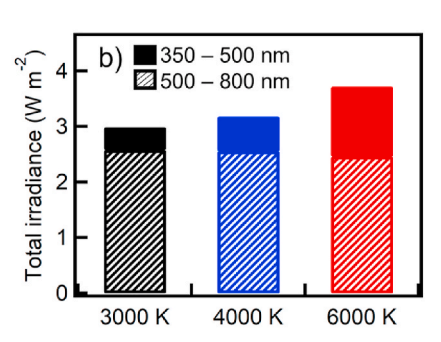


Fig. 2. (a) Spectral irradiances of LED light sources at three nominal CCTs: 3000 K (black), 4000 K (blue), and 6000 K (red). Each spectrum produces an illuminance of 1000 lx. (b) Bar chart of total irradiances of three spectra from Fig. 1(a). The solid-filled portions represent the irradiance integrated from 350 nm to 500 nm, and the hatch-patterned portions represent the irradiance integrated from 500 nm to 800 nm. (For interpretation of the references to color in this figure legend, the reader is referred to the Web version of this article.)

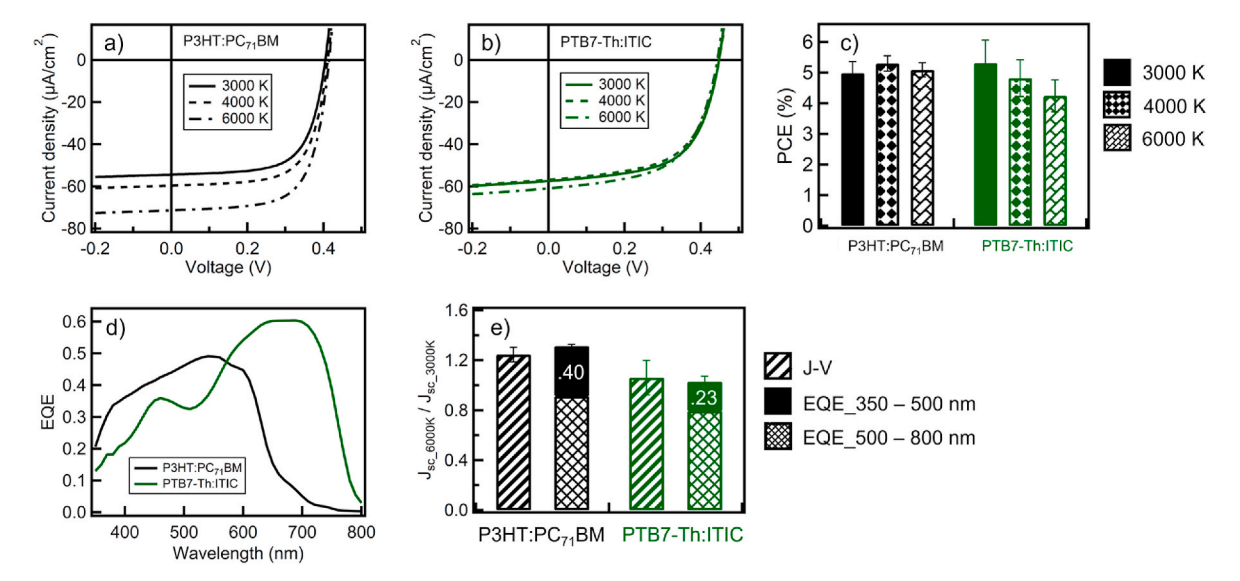


Fig. 3. J-V curves of (a) P3HT:PC₇₁BM and (b) PTB7-Th:ITIC BHJ devices under 1000 lx LED illumination at 3000 K (solid line), 4000 K (dashed line), and 6000 K (dashed and dotted line) CCTs. These J-V curves are averaged over at least 4 diodes. (c) PCEs for P3HT:PC₇₁BM (black) and PTB7-Th:ITIC (green) at 3000 K (solid filled), 4000 K (diamond), and 6000 K (diagonal brick). (d) External quantum efficiency (EQE) for P3HT:PC₇₁BM (black) and PTB7-Th:ITIC (green). (e) Bar chart of $J_{sc,6000 \text{ K}}/J_{sc,3000 \text{ K}}$ for P3HT:PC₇₁BM (black) and PTB7-Th:ITIC (green). (e) Bar chart of $J_{sc,6000 \text{ K}}/J_{sc,3000 \text{ K}}$ for P3HT:PC₇₁BM (black) and PTB7-Th:ITIC (green). (e) Bar chart of $J_{sc,6000 \text{ K}}/J_{sc,3000 \text{ K}}$ for P3HT:PC₇₁BM (black) and PTB7-Th:ITIC (green). (e) Bar chart of $J_{sc,6000 \text{ K}}/J_{sc,3000 \text{ K}}$ for P3HT:PC₇₁BM (black) and PTB7-Th:ITIC (green). (e) Bar chart of $J_{sc,6000 \text{ K}}/J_{sc,3000 \text{ K}}$ for P3HT:PC₇₁BM (black) and PTB7-Th:ITIC (b.23) using EQE $J_{sc}/J_{sc,800 \text{ K}}/J_{sc,800 \text{ K}}/J_{sc,800 \text{ K}}/J_{sc,8000 \text{ K}}/J_$

donors: poly(3-hexylthiophene) (P3HT), poly(5-bromo-4-(2-octyldodecyl)-selenophen2-yl)-5,6-difluorobenzothiadiazole-5,5'-bis-(trimethylstannyl)-2,2'-bithiophene (PFBT2Se2Th), poly[(2,6-(4,8-bis(5-(2ethylhexyl-3-fluoro)thiophen-2-yl)-benzo[1,2-b:4,5-b']dithiophene))alt-(5,5-(1',3'-di-2-thienyl-5',7'-bis(2-ethylhexyl)benzo[1',2'-c:4',5'-c'] dithiophene-4,8-dione)] (PM6), and poly{4,8-bis[5-(2-ethylhexyl)thiophen-2-yl]benzo[1,2-b:4,5-b']-dithiophene-2,6-diyl-alt-3-fluoro-2-[(2ethylhexyl)carbonyl]-thieno[3,4-b]thiophene-4,6-diyl} (PTB7-Th), and four acceptors [6,6]:-Phenyl-C71-butyric acid methyl ester (PC₇₁BM), 2, 2'Z)-((12,13-bis(2-ethylhexyl)-3,9-diundecyl-12,13-dihydro-[1,2,5]thiadiazolo[3,4-e]thieno[2",3":4',5"]thieno[2',3":4,5]pyrrolo[3, 2-g]thieno[2',3':4,5]thieno[3,2-b]indole-2,10-diyl)bis(methanylyliden e))bis(5,6-difluoro-3-oxo-2,3-dihydro-1H-indene-2,1-diylidene))dimalononitrile (Y6), 3,9-Bis(2-methylene-(3-(1,1-dicyanomethylene)-indanone))-5,5,11,11-tetrakis(4-hexylphenyl)-dithieno[2,3-d:2',3'-d']-s-indaceno[1,2-b:5,6-b']-dithiophene) (ITIC), and 2,2'-[[6,6,12,12-Tetrakis (4-hexylphenyl)-6,12-dihydrodithieno[2,3-d:2',3'-d']-s-indaceno[1, 2-b:5,6-b']dithiophene-2,8-diyl]bis[methylidyne(5,6-difluoro-3-oxo-1H-indene-2,1(3H)-diylidene)]]bis[propanedinitrile] (IT-4F). The energy levels of the neat materials, with bandgap energies extrapolated from Tauc plots (Fig. S1) and ionization energies measured from photoelectron spectroscopy in air (PESA), are shown in Fig. S2.

We built an experimental setup (Fig. S3a) based on Venkateswararao et al. [4] to test the IOPV performance under white LED illumination. After stabilizing the LED intensity (Fig. S3b), we adjust the LED intensity to achieve 1000 lx illuminance using a NIST-calibrated reference cell (Table S1). We use 1000 lx because it's the typical illumination level for well-lit office areas where 'cool white' illumination are often used [20]. Fig. 2a depicts the spectral irradiance of the LED source used in this study at nominal CCTs of 3000 K (black), 4000 K (blue), and 6000 K (red) taken at 1000 lx. The total irradiance calculated from integrating each curve is 2.99 W m $^{-2}$ at 3000 K, 3.18 W m $^{-2}$ at 4000 K, and 3.72 W m $^{-2}$ at 6000 K. The actual CCT values (Table S1) are determined from LED's relative spectral irradiances at different nominal CCTs (Fig. S3c). Fig. 2a shows that as CCT increases, the emission of the narrow peak at \approx 450 nm increases. To quantify this increasing optical power, we

calculate the irradiances in the blue (350 nm–500 nm, Fig. 2b solid bars) and red (500 nm–800 nm, Fig. 2b hatched bars) regions. While the irradiance in the blue region is the smaller portion of the total irradiance at each CCT (Fig. 2b), it increases from 0.41 W m $^{-2}$ at 3000 K, to 0.62 W m $^{-2}$ at 4000 K, and to 1.26 W m $^{-2}$ at 6000 K, while the irradiances in the red region are similar, 2.58 W m $^{-2}$ at 3000 K, 2.56 W m $^{-2}$ at 4000 K, and 2.46 W m $^{-2}$ at 6000 K. Therefore, the irradiance in the blue region increases modestly ($\approx\!50\%$) from 3000 K to 4000 K and significantly ($\approx\!100\%$) from 4000 K to 6000 K. Consequently, the irradiance in the blue region increases by $\approx\!200\%$ and the total irradiance increases by 30% from 3000 K to 6000 K. Thus, to achieve the same or higher PCE under 3000 K and 6000 K CCTs, the active layer must fully absorb the LED emission in the blue region.

In this study, we performed current density - voltage (J - V) measurements under LED 1000 lx illumination at nominal 3000 K, 4000 K, and 6000 K CCTs on IOPV devices with eight different absorbers (Fig. 1). The measured external quantum efficiency (EQE) spectra for all IOPV devices (Fig. S4), the LED emission spectra (Fig. 2), the reference spectral irradiance (Fig. S5a), and irradiance spectral responsivity for the reference cell (Fig. S5b) are used to calculate a spectral mismatch parameter (M, Table S2) based on Hamadani et al. [15]. All J - V curves shown in the paper have been corrected for spectral mismatch. All devices have been optimized to achieve good PV performance by doing optimization such as adding additives, selecting suitable host solvents for maximum solution solubility, adjusting solution dispensing procedure, varying active layer thickness, doing suitable active layer post-processing treatments (thermal and/or solvent annealing, annealing atmosphere), and choosing appropriate device structures (conventional or inverted architecture). Because this work focuses on the CCT behavior of various IOPV devices rather than on the absolute PCE values, it provides an excellent way to compare the device performance with different donor and acceptor combinations. Device parameters for all systems are summarized in Table S3.

To understand how the absorption in the blue region affects the J_{sc} under different nominal CCTs, we first compare P3HT:PC $_{71}BM$ and PTB7-Th:ITIC. Their J - V curves are shown in Fig. 3a,b. They are chosen

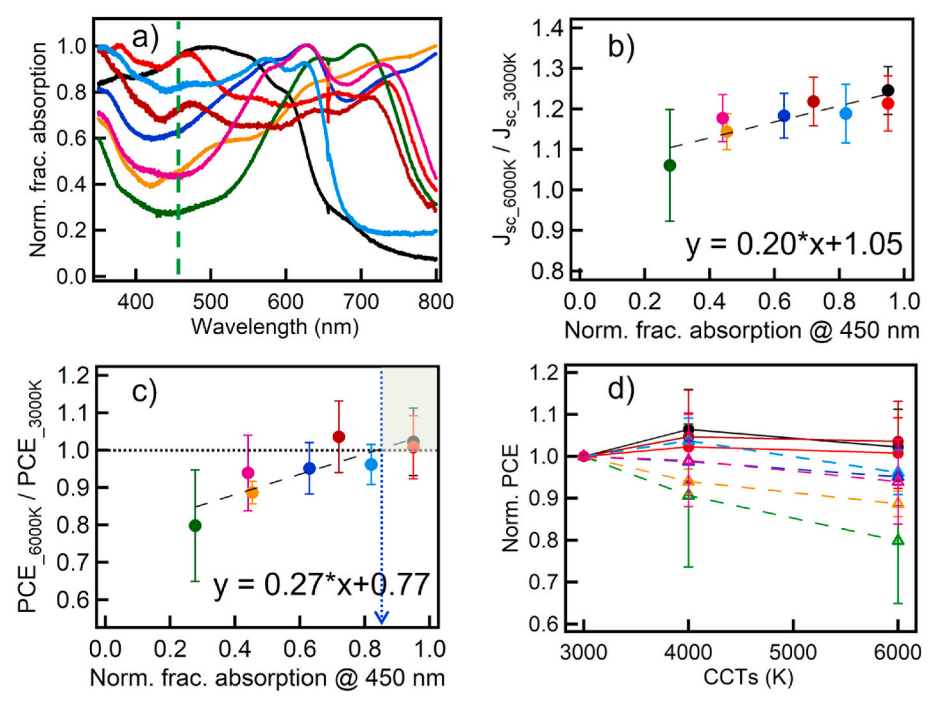


Fig. 4. (a) Norm-frac-abs spectra of P3HT:PC71BM (black), PFBT2Se2Th:PC71BM (red), PM6:PC71BM (light blue), PTB7-Th:PC71BM (maroon), PM6:Y6 (navy blue), 5 wt% PM6:Y6 (orange), PM6:IT-4F (magenta), and PTB7-Th:ITIC (green). The green dashed line indicates 450 nm, the blue emission peak for the LED. (b) $J_{sc\ 6000\ K}/J_{sc\ 3000\ K}$ vs. Norm-fracabs 450 nm. The black dashed line is a linear fit to the data. (c) PCE 6000 K/PCE 3000 K vs. Norm-frac-abs_450 nm. The black dashed line is a linear fit to the data. The intercept between $PCE_{\underline{6000 \text{ K}}}/PCE_{\underline{3000 \text{ K}}} = 1$ (black dotted line) and the linear fit occurs at Normfrac-abs 450 nm = 0.85. The light green shaded area represents the condition when PCE 6000 K/PCE 3000 K is greater than 1. (d) Normalized PCEs for all eight active laver systems under 1000 lx LED illumination at nominal 3000 K, 4000 K, and 6000 K CCTs. Three active layers show PCEs independent of CCTs (filled circles and solid lines): P3HT:PC71BM, PFBT2Se2Th: PC71BM, and PTB7-Th:PC71BM. The rest show lower PCEs at higher CCTs (open triangles and dashed lines): PM6:PC71BM, PM6:Y6, 5 wt% PM6:Y6, PM6: IT-4F, and PTB7-Th:ITIC. Uncertainty values in Fig. 4(b-d) show the mean and standard deviations of the results from at least 4 measurements. (For interpretation of the references to color in this figure legend, the reader is referred to the Web version of this article.)

based on two criteria. First, P3HT:PC71BM absorbs strongly in the blue region, while PTB7-Th:ITIC absorbs poorly in the same region (Figs. S6a and b)). P3HT:PC71BM shows an approximately three times higher absorption than PTB7-Th:ITIC in the blue region because the P3HT donor and the PC71BM acceptor have much stronger absorption below 500 nm than PTB7-Th and ITIC, respectively (Figs. S6c and d). Second, the J_{sc} and PCE values are similar under 3000 K CCT (Table S3), so it is more straightforward to study their changes from 3000 K to 6000 K CCT. The J_{sc} of P3HT:PC₇₁BM devices increases by 25%, from 54.3 μ A/cm² under 3000 K to 67.7 μ A/cm² under 6000 K, while the J_{sc} of PTB7-Th:ITIC devices is slightly higher by 6.1% as CCT increases (from 57.4 μA/cm² under 3000 K to $60.9 \,\mu\text{A/cm}^2$ under $6000 \,\text{K}$). Both types of devices have open-circuit voltage (Voc) and fill factor (FF) values independent of CCTs (Table S3). Thus, their performance as a function of CCT is determined by the J_{sc} trend. The PCE value of P3HT:PC71BM devices increases from 5.0% under 3000 K to 5.1% under 6000 K while that of PTB7-Th:ITIC devices decreases from 5.3% under 3000 K to 4.2% under 6000 K (Fig. 3c).

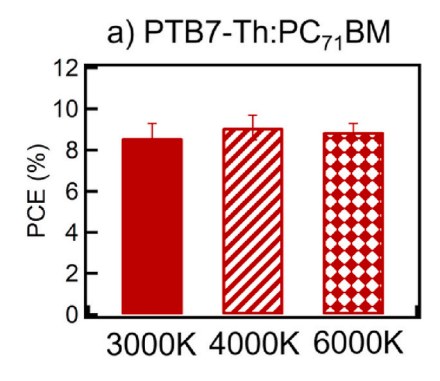
Fig. 3d shows EQE spectra for P3HT:PC₇₁BM and PTB7-Th:ITIC BHJ devices. P3HT:PC₇₁BM exhibits a strong photo-response from 350 nm to 600 nm, consistent with its Norm-frac-abs in Fig. S6a. PTB7-Th:ITIC shows a low photo-response in the blue region and a high photoresponse from 500 nm to 800 nm with a maximum EQE value peak at \approx 700 nm, consistent with its Norm-frac-abs in Fig. S6b. From EQE spectra, we can calculate J_{sc} and compare to the values from J - V measurements. Fig. 3e shows the ratio of J_{sc} between 3000 K and 6000 K $(J_{sc\ 6000\ K}/J_{sc\ 3000\ K})$ using J_{sc} values obtained from J - V and EQE measurements. For P3HT:PC71BM, by integrating the EQE spectrum from 350 nm to 800 nm using the LED spectra (Fig. 2a), the J_{sc 6000 K}/ $J_{sc\;3000\;K}$ value is 1.3, which agrees with its $J_{sc\;6000\;K}/J_{sc\;3000\;K}$ value from J-V measurement. For PTB7-Th:ITIC, the $J_{sc_6000~K}/J_{sc_3000~K}$ value from EQE spectrum is 1.0, well-matched with its $J_{sc_6000\ K}/J_{sc_3000\ K}$ value from J-V measurement. Since EQE is spectrally resolved, we can separate the J_{sc} contributions into blue (350 nm-500 nm) and red (500 nm–800 nm) spectral regions and calculate their $J_{sc_6000K}/J_{sc_3000\ K}$ values. These $J_{sc_6000\ K}/J_{sc_3000\ K}$ values are shown in Fig. 3e as solid for the blue region and cross grid for the red region. A noticeably larger contribution to the $J_{sc_6000~K}/J_{sc_3000~K}$ ratio from the blue region (350 nm-500 nm) is observed for P3HT:PC71BM, with $J_{sc_6000~K}$ (blue)/

 $J_{sc_3000~K}$ of 0.40, which is approximately two times higher than that for PTB7-Th:ITIC. In contrast, the difference in the contribution from 500 nm to 800 nm light to $J_{sc_6000~K}/J_{sc_3000~K}$ ratios is negligible for the two active layers. Therefore, a two-fold larger J_{sc} increase in 350 nm–500 nm region is the dominant factor for the higher J_{sc} observed in the photovoltaic performance of P3HT:PC $_{71}$ BM devices (Fig. 3a), highlighting the importance of active layer absorption in the blue region regarding to changes in CCTs.

To validate the above finding that CCT behavior of IOPV devices is determined by the active layer absorption in the blue region, we test IOPV devices based on six additional organic absorbers. The active layers are five BHJs: PFBT2Se2Th:PC71BM, PM6:PC71BM, PTB7-Th: PC₇₁BM, PM6:Y6, and PM6:IT-4F, and one dilute donor: 5 wt% PM6:Y6. Fig. 4a shows the Norm-frac-abs spectra for all eight absorber systems. The green dashed line marks 450 nm, the wavelength of the LED emission peak in the blue region in Fig. 2a. The Norm-frac-abs value at 450 nm (Norm-frac-abs 450 nm) for these 8 active layers vary from 0.2 to 1.0. The J - V curves under one-sun AM 1.5G are shown in Fig. S7 and the J - V curves for 1000 lx LED illumination at 3000 K, 4000 K, and 6000 K CCTs are shown in Fig. 3a,b and Fig. S8. The device parameters are summarized in Table S3. Fig. 4b shows the average $J_{sc_6000~\text{K}}/J_{sc_3000}$ K ratio increases linearly with Norm-frac-abs_450 nm (black dashed line in Fig. 4b). Our results show that the higher the active layer's Norm-fracabs 450 nm, the larger the J_{sc} increase under higher CCTs.

Both V_{oc} and FF values of all studied devices are independent of CCTs (Table S3), so PCE values are determined by the changes in J_{sc} . However, since the total irradiance also increases as CCTs increases, a higher J_{sc} at a higher CCT does not necessarily translate to a higher PCE. To study how the Norm-frac-abs_450 nm affects PCEs under different CCTs, we calculate the PCE_6000 $_{K}$ /PCE_3000 $_{K}$ ratio for all the devices as a function of Norm-frac-abs_450 nm (Fig. 4c). The PCE_6000 $_{K}$ /PCE_3000 $_{K}$ ratio also increases linearly with Norm-frac-abs_450 nm. For Norm-frac-abs_450 nm \geq 0.85, Fig. 4c shows that the PCE_6000 $_{K}$ /PCE_3000 $_{K}$ ratio reaches 1. We observe the same elimination of the PCE drop from 3000 $_{K}$ to 4000 $_{K}$ CCT (Fig. S9b). Therefore, Norm-frac-abs_450 nm is an important indicator of how a device would perform at 4000 $_{K}$ or 6000 $_{K}$ compared with at 3000 $_{K}$.

Fig. 4d shows the CCT dependence of the normalized PCE for all eight active layer systems. Clearly there are two groups: one with PCEs



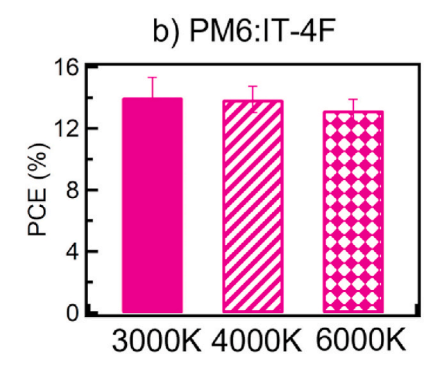


Fig. 5. Bar charts of PCEs for (a) PTB7-Th:PC₇₁BM and (b) PM6:IT-4F under 1000 lx LED illumination at 3000 K (solid-filled bars), 4000 K (hatched bars), and 6000 K (diamond-filled bars) CCTs. Uncertainty values in Fig. 5 show the mean and standard deviations of the results from at least 5 measurements.

independent of CCTs (solid lines and symbols) and one with diminishing PCEs at higher CCTs (dashed lines and open symbols). PTB7-Th:PC71BM devices produce the highest PCEs of 9.1% compared to other CCTagnostic systems, i.e., those with high Norm-frac-abs_450 nm values. P3HT:PC71BM and PFBT2Se2Th:PC71BM produce PCEs of 5.3% and 6.6%, respectively. The PTB7-Th:PC71BM devices exhibit CCTindependent V_{oc} and FF values of 0.58 V and 0.58, respectively, while the J_{sc} increases by 22% from 78.4 $\mu A/cm^2$ for 3000 K to 95.4 $\mu A/cm^2$ for 6000 K. The magnitude of J_{sc} increase is comparable to the total irradiance increase, 30%, from 3000 K to 6000 K. This system is an example of how the increase in \boldsymbol{J}_{sc} balances out that of total irradiance, leading to similar PCEs at different CCTs. In the group with decreasing PCEs at 6000 K, the three active layers that contain PM6 donors, PM6: PC₇₁BM, PM6:Y6, and PM6:IT-4F, show the smallest PCE reduction, 5%, from 3000 K to 6000 K. However, 5 wt% PM6:Y6 and PTB7-Th:ITIC exhibit much larger PCE reductions, 11% and 20%, respectively. The PM6:IT-4F devices show the highest PCEs of 14% at 3000 K compared to all other systems studied. The V_{oc} and FF values of PM6:IT-4F devices are independent across all CCTs, 0.64 V and 0.71, respectively. However, the J_{sc} values of PM6:IT-4F devices increases by 18% from 91.8 μ A/cm² under 3000 K to 108 μ A/cm² under 6000 K, resulting in slightly decreasing PCEs from 3000 K to 6000 K. Fig. 5 shows bar charts of PCEs for PTB7-Th:PC71BM and PM6:IT-4F at 3000 K, 4000 K, and 6000 K CCTs. The PCEs of PTB7-Th:PC71BM devices are similar, \approx 8.9%, for all CCTs (Fig. 5a), while the PCEs for PM6:IT-4F devices show a decreasing trend from 14.0% at 3000 K to 13.2% at 6000 K (Fig. 5b). Therefore, for applications that desire CCT-independent performance, PTB7-Th: PC₇₁BM devices should be chosen while for applications that demand the highest performance at 3000 K, PM6:IT-4F is the best candidate.

3. Conclusion

In conclusion, our results unambiguously show that the normalized fractional absorption value of the organic active layer at 450 nm can be used to forecast J_{sc} and PCE variation under white LED illumination with different CCTs. We find that $J_{sc_6000K}/J_{sc_3000\ K}$ and PCE_ $_{6000\ K}/PCE_{_{3000\ K}}$ ratios increase linearly as a function of Norm-frac-abs_450 nm. To avoid a PCE decrease going from 3000 K to 6000 K requires the Norm-fracabs 450 nm to be at least 0.85. Of the eight organic absorbers we investigated, PTB7-Th:PC71BM devices are the best performing IOPVs without PCE drop from 3000 K to 6000 K. In contrast, PM6:IT-4F devices can deliver more power at 3000 K, so they should be used in 'warm white' situations. IOPV devices with higher performance than this work have been reported in the literature. However, the CCT behavior is robust regardless of the absolute PCE values and can be predicted based on the Norm-frac-abs_450 nm of the absorber. Our result provides a guidance on molecular design to achieve CCT-independent IOPVs with high performance [21].

Declaration of competing interest

The authors declare that they have no known competing financial interests or personal relationships that could have appeared to influence the work reported in this paper.

Acknowledgements

We would like to thank Z. Ma for drawing chemical structures. This project is supported by National Science Foundation CBET-1916612, United States and The UT Dallas Seed Program for Interdisciplinary Research (SPIRe), United States. J.W.P.H acknowledges the Texas Instruments Distinguished Chair in Nanoelectronics, United States.

Appendix A. Supplementary data

Supplementary data to this article can be found online at https://doi.org/10.1016/j.orgel.2022.106477.

References

- [1] T. Kim, C. Ramos, S. Mohammed, Smart city and IoT, Future Generat. Comput. Syst. 76 (2017) 159–162, https://doi.org/10.1016/j.future.2017.03.034.
- [2] M. Shirvanimoghaddam, K. Shirvanimoghaddam, M.M. Abolhasani, M. Farhangi, V.Z. Barsari, H. Liu, M. Dohler, M. Naebe, Paving the path to a green and selfpowered Internet of Things, ArXiv Prepr, 2017, pp. 1–24, arXiv:1712.02277v1.
- [3] J.M. Gilbert, F. Balouchi, Comparison of energy harvesting systems for wireless sensor networks, Int. J. Autom. Comput. 5 (2008) 334–347, https://doi.org/ 10.1007/s11633-008-0334-2.
- [4] A. Venkateswararao, J.K.W. Ho, S.K. So, S.W. Liu, K.T. Wong, Device characteristics and material developments of indoor photovoltaic devices, Mater. Sci. Eng. R Rep. 139 (2020) 100517, https://doi.org/10.1016/j. mser 2019 100517
- [5] S. Biswas, H. Kim, Solar cells for indoor applications: progress and development, Polymers 12 (2020) 1338, https://doi.org/10.3390/POLYM12061338.
- [6] A.K. Chauhan, P. Kumar, Degradation in perovskite solar cells stored under different environmental conditions, J. Phys. D Appl. Phys. 50 (2017) 325105, https://doi.org/10.1088/1361-6463/aa7905.
- [7] I. Mathews, S.N. Kantareddy, T. Buonassisi, I.M. Peters, Technology and market perspective for indoor photovoltaic cells, Joule 3 (2019) 1415–1426, https://doi. org/10.1016/j.joule.2019.03.026.
- [8] M.A. Saeed, S.H. Kim, H. Kim, J. Liang, H.Y. Woo, T.G. Kim, H. Yan, J.W. Shim, Indoor organic photovoltaics: optimal cell design principles with synergistic parasitic resistance and optical modulation effect, Adv. Energy Mater. 11 (2021) 2003103. https://doi.org/10.1002/anm.202003103.
- [9] L. Xie, W. Song, J. Ge, B. Tang, X. Zhang, T. Wu, Z. Ge, Recent progress of organic photovoltaics for indoor energy harvesting, Nano Energy 82 (2021) 105770, https://doi.org/10.1016/i.nanoen.2021.105770.
- [10] H.S. Ryu, S.Y. Park, T.H. Lee, J.Y. Kim, H.Y. Woo, Recent progress in indoor organic photovoltaics, Nanoscale 12 (2020) 5792–5804, https://doi.org/10.1039/ d0nr00816h.
- [11] Y. Cui, L. Hong, J. Hou, Organic photovoltaic cells for indoor applications: opportunities and challenges, ACS Appl. Mater. Interfaces 12 (2020) 38815–38828, https://doi.org/10.1021/acsami.0c10444
- [12] M. Ylikunnari, M. Välimäki, K.L. Väisänen, T.M. Kraft, R. Sliz, G. Corso, R. Po, R. Barbieri, C. Carbonera, G. Gorni, M. Vilkman, Flexible OPV modules for highly efficient indoor applications, Flex. Print. Electron. 5 (2020), 014008, https://doi.org/10.1088/2058-8585/ab6e73.

- [13] P. Alstone, A. Jacobson, LED advances accelerate universal access to electric lighting, Compt. Rendus Phys. 19 (2018) 146–158, https://doi.org/10.1016/j. crbv 2017 10 015
- [14] B. Gayral, LEDs for lighting: basic physics and prospects for energy savings, Compt. Rendus Phys. 18 (2017) 453–461, https://doi.org/10.1016/j.crhy.2017.09.001.
- [15] B.H. Hamadani, M.B. Campanelli, Photovoltaic characterization under artificial low irradiance conditions using reference solar cells, IEEE J. Photovoltaics. 10 (2020) 1119–1125, https://doi.org/10.1109/JPHOTOV.2020.2996241.
- [16] A.R. Robertson, Computation of correlated color temperature and distribution temperature, J. Opt. Soc. Am. 58 (1968) 1528–1535, https://doi.org/10.1364/ JOSA.58.001528.
- [17] H. Yin, J.K.W. Ho, S.H. Cheung, R.J. Yan, K.L. Chiu, X. Hao, S.K. So, Designing a ternary photovoltaic cell for indoor light harvesting with a power conversion efficiency exceeding 20%, J. Mater. Chem. A. 6 (2018) 8579–8585, https://doi. org/10.1039/c8ta01728j.
- [18] S. Lee, H.C. Yoon, A randomized controlled trail for comparing LED color temperature and color rendering attributes in different illuminance environments for human-centric office lighting, Appl. Sci. 11 (2021) 8313, https://doi.org/ 10.3390/appl.1188313
- [19] Q. Wang, H. Xu, F. Zhang, Z. Wang, Influence of color temperature on comfort and preference for LED indoor lighting, Optik 129 (2017) 21–29, https://doi.org/ 10.1016/j.ijleo.2016.10.049.
- [20] I. Mathews, G. Kelly, P.J. King, R. Frizzell, GaAs solar cells for indoor light harvesting, in: IEEE 40th Photovolt. Spec. Conf. PVSC, 2014, pp. 510–513, https://doi.org/10.1109/PVSC.2014.6924971.
- [21] Certain commercial equipment, instruments, software, or materials are identified in this paper to specify the experimental procedure adequately. Such identification is not intended to imply recommendation or endorsement by the National Institute of Standards and Technology nor is it intended to imply that the materials or equipment identified is necessarily the best available for the purpose.